www.lajss.org
Latin American Journal of Solids and Structures 2 (2005) 253–267

FE analysis of reinforced concrete beams strengthened by composite plates

Roberto C. Pavan*, Branca F. Oliveira and Guillermo J. Creus

CEMACOM-PPGEC-UFRGS
Av. Osvaldo Aranha, 99, 90035-190, Porto Alegre, RS – Brazil

Abstract

In this work, a computational model for the simulation of the behavior of structures of composite materials is presented. The formulation includes elastic anisotropic relations, viscoelastic anisotropic constitutive equations in terms of state variables, failure and plastic criteria, all in a setting of large displacements with small strains. The equations are set in a form adequate for numerical analysis through the finite element method, using degenerate three-dimensional shell elements and an incremental-iterative procedure accounting for post-critical effects. Some examples of application are shown. The main examples analyze reinforced concrete beams strengthened for flexure by composite plates and present a comparison with experimental results.

Keywords: composite materials, finite elements, viscoelasticity, plasticity, failure.

1 Introduction

Nowadays there is a great interest in the reinforcement and recovery of structures through the use of composite materials. Reinforcement is necessary when the structure will be submitted to a loading condition different of that for which it was projected. Recovery is related to situations where, due the deterioration of the structure, its original load capacity must be restituted (see for example [6, 7, 11, 16]).

The use of composites has advantages in situations of reinforcement and recovery because of their high stiffness/weight ratio and strength/weight ratio (composites strengthened for carbon fiber, for example, possess stiffness ratios 10-15 times higher than steel), excellent resistance to corrosion, low thermal expansion, good performance in fatigue and tolerance to damage, easiness of transport and conservation, possibility of inclusion of "strain gages" inside the structure for a continuous control, low consumption of energy in the manufacture process of the material and the structure [2]. Thus, the use of the composites provides strength and stiffness without an expressive increase of self weight.

*Corresp. author Email: pavan@ppgec.ufrgs.br Received 23 September 2005; In revised form 18 October 2005

In this work, a computational procedure primarily developed for composite materials structure analysis is presented. It is shown that, with some additions and modifications, the procedure can be extended to concrete structures reinforced with composite material.

In section 2 the finite elements model is presented. In section 3 the model for viscoelasticity of the material is described. In section 4 the procedure for numerical solution of the incremental equations is presented. In sections 5 and 6 the progressive failure and plasticity models are described. In section 7 some examples are shown and compared with experimental results. In section 8 conclusions and final remarks are presented.

2 Finite Element Model

The expression of the virtual displacement principle in a total Lagrangian formulation may be written as [3]

$$\int_{{}_0V} {}^{k+1}_{0}S_{ij}\delta\, {}^{k+1}_{0}\varepsilon_{ij}\, {}^{0}\mathrm{d}V = {}^{\mathrm{k+1}}R \tag{1}$$

where ${}^{k+1}R$ is the virtual work of external forces in the *(k+1)th* incremental step, ${}^{k+1}_{0}S_{ij}$, ${}^{k+1}_{0}\varepsilon_{ij}$ are components of the second Piola-Kirchhoff stress tensor and Green-Lagrange strain tensor in the *(k+1)th* step, respectively, both referred to the initial configuration, and ${}^{0}V$ is the initial configuration volume of the body.

We may write ${}^{k+1}_{0}S_{ij} = {}^{k}_{0}S_{ij} + {}_0S_{ij}$, ${}^{k+1}_{0}\varepsilon_{ij} = {}^{k}_{0}\varepsilon_{ij} + {}_0\varepsilon_{ij}$ where ${}_0S_{ij}$ and ${}_0\varepsilon_{ij}$ are the increments in stress and strain components, respectively, in the *(k+1)th* step. The strain increment may still be decomposed into linear ${}_0e_{ij}$ and nonlinear ${}_0\eta_{ij}$ parts as ${}_0\varepsilon_{ij} = {}_0e_{ij} + {}_0\eta_{ij}$.

Writing the strain increments decomposed into instantaneous, deferred, thermal and hygroscopic components we have

$${}_0\varepsilon_{ij} = {}_0\varepsilon^{e}_{ij} + {}_0\varepsilon^{y}_{ij} + {}_0\varepsilon^{T}_{ij} + {}_0\varepsilon^{H}_{ij} \tag{2}$$

The linearized relation between stress and strain increments may then be written as [3]

$${}_0S_{ij} = {}_0C_{ijrs}[{}_0e_{rs} - {}_0e^{r}_{rs} - {}_0e^{T}_{rs} - {}_0e^{H}_{rs}] \tag{3}$$

Using the previous equations, we obtain

$$\begin{aligned} &\textstyle\int_{{}_0V} {}_0C_{ijrs}{}_0e_{rs}\delta_0 e_{ij}\, {}^{0}dV + \int_{{}_0V} {}^{k}_{0}S_{ij}\delta_0\eta_{ij}\, {}^{0}dV = \\ &= {}^{k+1}R - \textstyle\int_{{}_0V} {}^{k}_{0}S_{ij}\delta_0 e_{ij}\, {}^{0}dV + \int_{{}_0V} {}_0C_{ijrs}{}_0e^{v}_{rs}\delta_0 e_{ij}\, {}^{0}dV + \\ &+ \textstyle\int_{{}_0V} {}_0C_{ijrs}({}_0e^{T}_{rs} + {}_0e^{H}_{rs})\delta_0 e_{ij}\, {}^{0}dV \end{aligned} \tag{4}$$

Working with the finite element method and using matrix notation, the above equation may be written for each element

$$\begin{aligned} &\left[\textstyle\int_{{}_0V} \left[{}^{k}_{0}B_L\right]^T \; [{}_0C] \; \left[{}^{k}_{0}B_L\right] \; {}^{0}dV + \int_{{}_0V} \left[{}^{k}_{0}B_{NL}\right]^T \; \left[{}^{k}_{0}S\right] \; \left[{}^{k}_{0}B_{NL}\right] \; {}^{0}dV\right] \; \{U\} = \\ &= \left\{{}^{\mathrm{k+1}}R\right\} - \textstyle\int_{{}_0V} \left[{}^{k}_{0}B_L\right]^T \; \left\{{}^{k}_{0}S\right\} \; {}^{0}dV + \int_{{}_0V} \left[{}^{k}_{0}B_L\right]^T \; [\partial \mathrm{C}] \; \left(\left\{{}^{0}e^{v}\right\} + \left\{{}^{0}e^{T}\right\} + \left\{{}^{0}e^{H}\right\}\right) \; {}^{0}dV \end{aligned} \tag{5}$$

where {U} is the local displacement increment vector, $[{}^k_0 B_L]$ and $[{}^k_0 B_{NL}]$ are the linear and nonlinear strains-displacement transformation matrices, respectively and $[\,]^T$ indicates the transpose of a matrix. (For more details on these last matrices, see [3, 15, 18]).

Evaluating the volume integrals on each of the N layers of volume V_q we may write

$$\left(\left[{}^k_0 K_L\right] + \left[{}^k_0 K_{NL}\right]\right)\{U\} = \left\{{}^{k+1}P\right\} - \left\{{}^k_0 F\right\} + \{{}_0F^v\} + \left\{{}_0F^T\right\} + \left\{{}_0F^H\right\} \tag{6}$$

being

$$\left[{}^k_0 K_L\right] = \sum_{q=1}^{N} \int_{{}_0V_q} \left[{}^k_0 B_L\right]^T \; [{}_0C] \; \left[{}^k_0 B_L\right] \; {}^0dV_q \tag{7}$$

$$\left[{}^k_0 K_{NL}\right] = \sum_{q+1}^{N} \int_{{}_0V_q} \left[{}^k_0 B_{NL}\right]^T \; \left[{}^k_0 S\right] \; \left[{}^k_0 B_{NL}\right] \; {}^0dV_q \tag{8}$$

$$\left\{{}^k_0 F\right\} = \sum_{q=1}^{N} \int_{{}_0V_q} \left[{}^k_0 B_L\right]^T \; \left\{{}^k_0 S\right\} \; {}^0dV_q \tag{9}$$

$$\{{}_0F^v\} = \sum_{q=1}^{N} \int_{{}_0V_q} \left[{}^k_0 B_L\right]^T \; [{}_0\mathrm{C}] \; \{{}_0e^v\} \; {}^0dV_q \tag{10}$$

$$\left\{{}_0F^T\right\} = \sum_{q=1}^{N} \int_{{}_0V_q} \left[{}^k_0 B_L\right]^T \; [{}_0\mathrm{C}] \; \left\{{}_0e^T\right\} \; {}^0dV_q \tag{11}$$

$$\left\{{}_0F^H\right\} = \sum_{q=1}^{N} \int_{{}_0V_q} \left[{}^k_0 B_L\right]^T \; [{}_0\mathrm{C}] \; \left\{{}_0e^H\right\} \; {}^0dV_q \tag{12}$$

In the expressions above, $\left[{}^k_0 K_L\right]$ and $\left[{}^k_0 K_{NL}\right]$ are the linear and nonlinear tangent stiffness matrices, respectively, corresponding to step k, $\left\{{}^{k+1}P\right\}$ is the vector of the external nodal forces at step $(k+1)$, $\left\{{}^k_0 F\right\}$ is the vector of nodal point forces equivalent to the element stresses at the step k and, finally, $\{{}_0F^v\}$,$\left\{{}_0F^T\right\}$ and $\left\{{}_0F^H\right\}$ are the vectors of viscoelastic, thermal and hygroscopic loads, respectively.

In the present formulation isoparametric tridimensional element degenerated into a shell element is used [10]. The element has five degrees of freedom per node, three translations $(u_x, u_y, u_z)$and two in-surface rotations (ϕ_x, ϕ_y). Four, eight and nine node elements have been implemented with the possibility to use normal or reduced integration rules. Gauss points are distributed in the layers of the elements. Accuracy tests for this code are shown in [18].

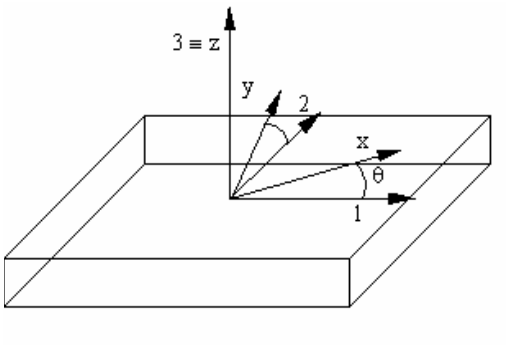

Figure 1: Coordinate systems of an anisotropic layer

3 Viscoelastic Material Modeling

Figure 1 shows an orthotropic linear viscoelastic layer for which the principal material directions are coincident with the axes 1, 2 and 3. For mechanical and hygrothermal loads, the constitutive relations of the layer, referred to the principal material directions, may be written as

$$\varepsilon_i(t) = \int_0^t D_{ij}(T,H,t-\tau)\frac{\partial \sigma_j(\tau)}{\partial \tau}d\tau \; + \int_{T^*}^{T} \alpha_i(T,H)\; dT + \; \int_{H^*}^{H} \beta_i(T,H)\; dH \qquad \text{i, j} = 1, ...5 \tag{13}$$

where $\varepsilon_i\,(t)$ and $\sigma_j\,(t)$ are the components of the strain vector $\{\varepsilon\} = \{\varepsilon_{11},\ \varepsilon_{22},\ 2\varepsilon_{12},\ 2\varepsilon_{13},\ 2\varepsilon_{23}\}$ and stress vector $\{\sigma\} = \{\sigma_{11},\ \sigma_{22},\ \sigma_{12},\ \sigma_{13},\ \sigma_{23}\}$, at time t. The components ε_{33} and σ_{33} are not considered here. T and H indicate the temperature and moisture content.. In (13), $D_{ij}(T,\ H,\ \mathrm{t}-\tau)$ are the creep functions corresponding to components ε_i and σ_j, $\alpha_i(T,\ H)$ are the thermal expansion coefficients, $\beta_i(T,\ H)$ are the hygroscopic expansion coefficients, that in general depend on moisture content and temperature. T^* and H^* are the temperature and moisture values corresponding to the strain-free state. ε_i, σ_j, T and H are field variables and thus change in general from point to point, even when this dependence is not explicitly stated.

At this point we assume the material to be hygrothermal-rheologically simple, and therefore we write $D_{ij}(T,\ H,\ T) = D_{ij}(T_0,\ H_0,\ \xi_{ij})$ where T_0 and H_0 are reference values, and $\xi_{ij}$are the reduced times. Then,

$$\varepsilon_i = \int_0^t D_{ij}(T_0,\ H_0,\ \xi_{ij}-\xi'_{ij})\ \frac{\partial \sigma_j(\tau)}{\partial \tau}\ d\tau \ + \ \int_{T^*}^{T} \alpha_i(T,\ H)\ dT + \ \int_{H^*}^{H} \beta_i(T,\ H)\ dH \tag{14}$$

where $\xi_{ij} = \int_0^t \varphi_{ij}\left[T\left(\tau\right), H\left(\tau\right) d\tau\right]$, $\xi'_{ij} = \int_0^\tau \varphi_{ij}\left[T\left(s\right), H\left(s\right) ds\right]$, and φ_{ij} are temperature-moisture shift factors to be determined experimentally.

As we are concerned with small strains, we can decompose the total strain components ε_i into viscoelastic $\bar{\varepsilon}_i$ thermal ε_i^T and hygroscopic ε_i^H parts

$$\varepsilon_i(t) = \bar{\varepsilon}_i(t) + \varepsilon_i^T(T,\ H) + \varepsilon_i^H(T,\ H) \tag{15}$$

Upon integration by parts, the first integral in (14) may be written

$$\bar{\varepsilon}_{i}(t) = D_{ij}(T_0,\ H_0,\ 0)\ \sigma_j(t)\ -\ \int_{o}^{t} D_{ij}(T_0,\ H_0, \xi_{ij} - \xi'_{ij})\ \alpha_j(\tau)\ d\tau \tag{16}$$

Approximating the creep functions by a Dirichlet-Prony series we have

$$D_{ij}(T_0,\ H_0, \xi_{ij} - \xi'_{ij}) = D^0_{ij} + \sum_{p=1}^{M} D^p_{ij} \left[1 - \exp\left(-\frac{\xi_{ij} - \xi'_{ij}}{\theta^p_{ij}}\right)\right] \tag{17}$$

where D^0_{ij}, D^p_{ij} and θ^p_{ij} are parameters to be determined from experimental results. M is the number of significant terms in the series and depends on the accuracy desired. The parameters θ^p_{ij} are called retardation times.

Substituting (17) into (16) we have

$$\bar{\varepsilon}_{i}(t) = D_{ij}(T_0,\ H_0,\ 0)\sigma_j(t) + \sum_{p=1}^{M} \int_{0}^{t} d^p_{ij}(T_0,\ H_0,\ \xi_{\mathrm{ij}} - \xi'_{ij})\sigma_j(\tau)\ d\tau \tag{18}$$

where

$$d^p_{ij} = \frac{D^p_{ij}}{\theta^p_{ij}} \varphi_{ij} \exp\left(-\frac{\xi_{ij} - \xi'_{ij}}{\theta^p_{ij}}\right) \tag{19}$$

with no summation taking place on i, j. We may still write

$$\bar{\varepsilon}_{i}(t) = D_{ij}(T_0,\ H_0,\ 0)\sigma_j(t) + \sum_{p=1}^{M} \sum_{s=1}^{5} q^p_{is}(t) \tag{20}$$

It can be shown [18] that the $q^p_{is}(t)$ state variables are given by

$$\frac{\partial q^p_{is}}{\partial t} + \frac{q^p_{is}}{\theta^p_{is}} = \frac{D^p_{is}}{\theta^p_{is}} \sigma_i(t) \tag{21}$$

This is a system of linear first-order uncoupled differential equations that together with the initial condition $q^p_{ij} = 0$ at $t = 0$ allow the determination of the state variables knowing the stress history. This system may be solved incrementally by finite differences, as is indicated in the next section.

4 Numerical Solution

The numerical solution of the problem formulated in Sec. 2 and 3 is implemented through an incremental-iterative procedure. Thus, the nonlinear equilibrium equations (6) are written as

$$\left(\left[{}^{k+1}_{0}K_L\right]^{i-1} + \left[{}^{k+1}_{0}K_{NL}\right]^{i-1}\right)\{U\}^i = \left\{{}^{k+1}P\right\} - \left\{{}^{K+1}_{0}F\right\}^{i-1} + \left\{{}_0F^v\right\}^i + \left\{{}_0F^T\right\}^i + \left\{{}_0F^H\right\}^i \tag{22}$$

where the index i indicates the number of the iteration step. The viscoelastic, thermal and hygroscopic load vectors are taken as zero for $i \geq 2$. For $i = 1$, these vectors are determined by means of (10), (11) and (12), respectively.

For the solution of the nonlinear equilibrium equations (22), both Newton–Raphson and Generalized Displacement Control methods [23] have been implemented. In the Newton–Raphson method, a prescribed load increment is used. One limitation of this method is the numerical instability that occurs near the limit load when the stiffness matrix becomes singular. This inconvenient is avoided by the Generalized Displacement Control method (GDCM).

As for the time integration of state variables and considering a small time-interval Δt, we can write from (19) and (21)

$$q_{ij}^{p}(t+\Delta t) = \int_{0}^{t+\Delta t} \frac{D_{ij}^{p}}{\theta_{ij}^{p}} \varphi_{ij} \exp\left(-\frac{\xi_{ij} + \Delta\xi_{ij} - \xi'_{ij}}{\theta_{ij}^{p}}\right) \sigma_j(\tau)\, d\tau \tag{23}$$

Taking $\sigma(\tau)$ as constant along the interval Δt and equal to $\sigma(t)$, we can integrate to obtain

$$q_{ij}^{p}(t+\Delta t) = q_{ij}^{p}(t) \exp\left(-\frac{\Delta\xi_{ij}}{\theta_{ij}^{p}}\right) + D_{ij}^{p}\left\{1 - \exp\left(-\frac{\Delta\xi_{ij}}{\theta_{ij}^{p}}\right)\right\} \sigma_j(t) \tag{24}$$

Using (24), it is possible to evaluate the variables q_{ij}^{p}, at time $t+\Delta t$ as functions of their values at time t.

5 Failure Analysis

5.1 Progressive Failure Analysis

For the progressive failure analysis several criteria (Hashin [9], Lee [12,13], Maximum Strain [8]) have been implemented. To take into account material degradation, material stiffness reduction are introduced after the detection of the ply failures. In this work a simplified degradation model, which reduces particular terms in the material stiffness matrix, according to the failure mode, is used (see [5, 13, 18, 20]).

5.2 Maximum Strain Criteria

This criteria establishes that the failure occurs when one of the strain components, acting in the principal material directions, attains its limit value, which has to be determined by experimental tests. In the Maximum Strain Criteria failure happens when one of the conditions below are satisfied.

Extension

$$\left(\frac{\varepsilon_{11}}{X_{\varepsilon t}}\right)^2 = 1; \left(\frac{\varepsilon_{22}}{Y_{\varepsilon t}}\right)^2 = 1 \tag{25}$$

Shortening

$$\left(\frac{\varepsilon_{11}}{X_{\varepsilon c}}\right)^2 = 1; \left(\frac{\varepsilon_{22}}{Y_{\varepsilon c}}\right)^2 = 1 \tag{26}$$

Distortion

$$\left(\frac{\varepsilon_{12}}{S_{\varepsilon A}}\right)^2 = 1; \left(\frac{\varepsilon_{13}}{S_{\varepsilon A}}\right)^2 = 1; \left(\frac{\varepsilon_{23}}{S_{\varepsilon T}}\right)^2 = 1 \tag{27}$$

where

$X_{\varepsilon t}$– extension limit strain in the direction 1
$X_{\varepsilon c}$– shortening limit strain in the direction 1
$Y_{\varepsilon t}$– extension limit strain in the direction 2
$Y_{\varepsilon c}$– shortening limit strain in the direction 2
$S_{\varepsilon A}$– distortion limit strain in the plans 1-2 e 1-3
$S_{\varepsilon T}$– distortion limit strain in the plan 2-3

6 Plasticity Model for Steel

To simulate de behavior of reinforced beams and plates, the reinforcement is approximated by a layer of elasto-plastic material. For the plasticity analysis the criterion of von Mises is used. For Plane Stress, the yield condition is

$$Y = \sigma_{11}^2 + \sigma_{22}^2 - \sigma_{11}\sigma_{22} + 3\sigma_{12}^2 - \sigma_e^2 = 0 \tag{28}$$

The elastoplastic matrix is given by [19],

$$\mathrm{E}_{ep} = \mathrm{E} - \frac{\mathrm{E}\ \frac{\partial Y}{\partial \sigma}\left(\frac{\partial Y}{\partial \sigma}\right)^T \mathrm{E}}{H' + \left(\frac{\partial Y}{\partial \sigma}\right)^T \mathrm{E}\ \left(\frac{\partial Y}{\partial \sigma}\right)} \tag{29}$$

where

$\boldsymbol{E}$ - elastic constitutive matrix
$\boldsymbol{\sigma}$ - stress tensor
H' – strain hardening (in this work assumed to be zero)
Writing (29) in matrix form we get, for the case of plane stress:

$$\mathrm{E}_{ep} = \begin{bmatrix} \frac{E}{1-\nu^2} - \frac{S_1^2}{S_5} & \frac{E}{1-\nu^2}\nu - \frac{S_1\ S_2}{S_5} & -\frac{S_1\ S_3}{S_5} \\ \frac{E}{1-\nu^2}\nu - \frac{S_1\ S_2}{S_5} & \frac{E}{1-\nu^2} - \frac{S_2^2}{S_5} & -\frac{S_2\ S_3}{S_5} \\ -\frac{S_1\ S_3}{S_5} & -\frac{S_2\ S_3}{S_5} & \frac{E}{2(1+\nu)} - \frac{S_3^2}{S_5} \end{bmatrix} \tag{30}$$

where

$$S_1 = \frac{E}{1-\nu^2}\left(s_{11} + \nu\ s_{22}\right) \tag{31}$$

$$S_2 = \frac{E}{1-\nu^2}\left(\nu\ s_{11} + \ s_{22}\right) \tag{32}$$

$$S_3 = \frac{E}{1+\nu}\ s_{12} \tag{33}$$

$$S_4 = S_1\ s_{11} + S_2\ s_{22} + 2\ S_3\ s_{12} \tag{34}$$

$$S_5 = \frac{4}{9}H'\sigma_e^2 + S_4 \tag{35}$$

$$s_{ij} = \sigma_{ij} - \frac{1}{3}\left(tr\ \sigma_{ij}\right)\ \delta_{ij} \tag{36}$$

7 Examples

7.1 Analysis of an elastoplastic laminated plate in tension

The analyzed laminated plate is shown in Fig. 2(a) and 2(b). Layers 1 and 4 are constituted by a material with yield stress of 600MPa and layers 2 and 3 by a material with yield stress of 300 MPa. For both materials E = 200 GPa and ν = 0,3. The numerical result is shown in Fig. 2(c).

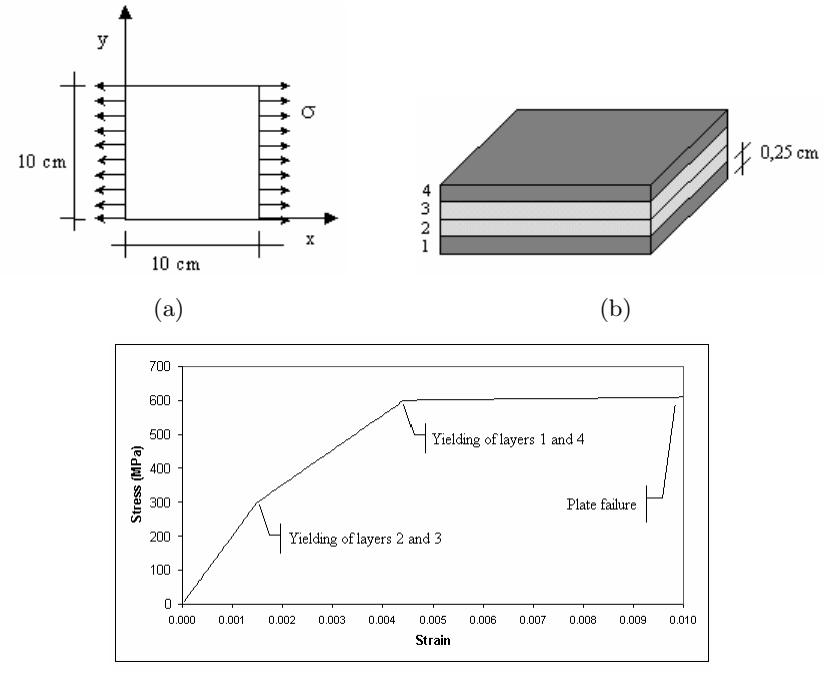

Figure 2: a) Geometry and loads; b) Lamination layout; c) Numerical result.

The yielding of layers (2,3) e (1,4) takes place at the expected stresses.

7.2 Analysis of a steel-concrete laminated plate in bending

This example deals with the analysis of a cantilever plate submitted to a constant bending moment as shown in Fig. 3(a). The plate is square with sides of 10 cm. For the material in the upper part (concrete) E = 20 GPa and for the material in the lower layer (steel) E=200GPa. To compare with a simple analytical solution, $\nu = 0$ was adopted.

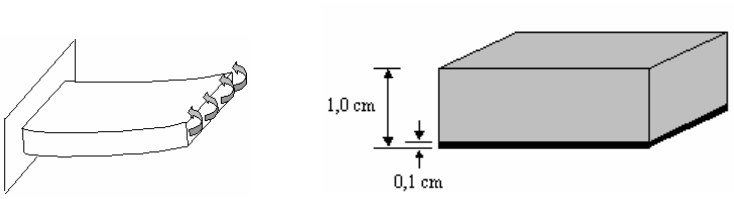

(a)

(b)

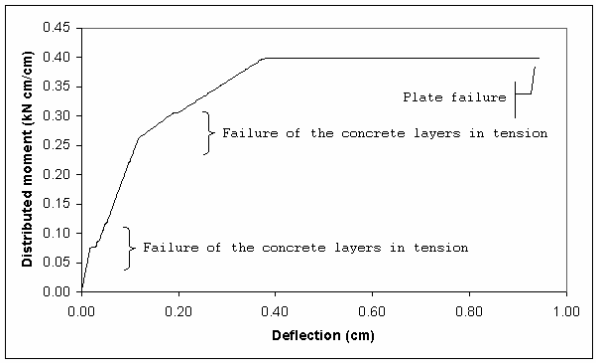

(c)

Figure 3: a) Cantilever plate submitted to bending; b) Concrete plate with a steel lower layer; c) Load-deflection plot at the free end.

For concrete, a tensile strength of 3 MPa and a compressive strength of 30 MPa, are used. The yield stress of steel is taken as 300 MPa. For the analysis of progressive failure the Hashin Criterion was used [9]. The concrete part is divided into ten layers. The results are presented in Fig. 3(c). In the graph, the stiffness reduction due to failure of the tensile layers of concrete can be observed; when the steel layer yields, the limit load is reached.

7.3 Analysis of a reinforced concrete beam strengthened by composite material plates

In this example the analysis of T-section reinforced concrete beam strengthened by CFRP plates is presented. For the progressive failure analysis the Maximum strain criterion was used and

the results had been compared with those in [22]. Fig. 4 shows beam geometry and cross section. Fig. 5 shows the form of loads application. The steel bars are represented by plates with equivalent cross-section area. The laminated shell elements used here have been also tested to model thin walled composite beams [17]. The used mesh has 60 eight node elements and 227 nodes.

The materials properties are as follows:

- Concrete: E = 21 GPa, ultimate strain = 0.3%.
- Upper steel: E= 197 GPa, yield stress = 316 MPa.
- Lower steel: E= 192 GPa, yield stress = 325 MPa .
- Carbon fiber reinforced polymeric material - CFRP [14]: E= 65 GPa, ultimate strain = 1%.

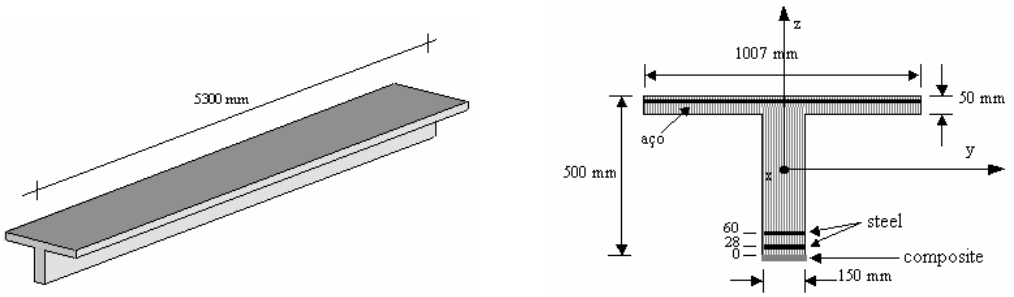

(a) (b)

Figure 4: T-beam a) Geometry b) Cross Section

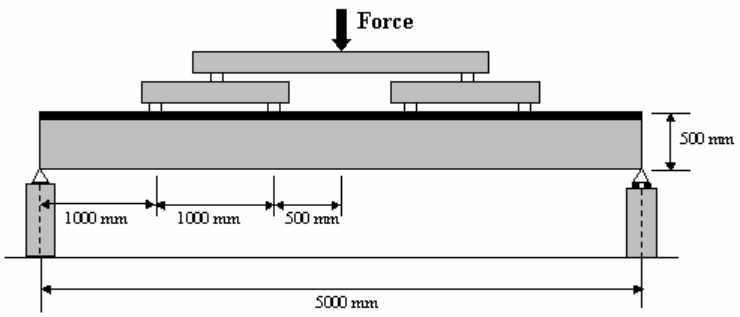

Figure 5: Experimental layout

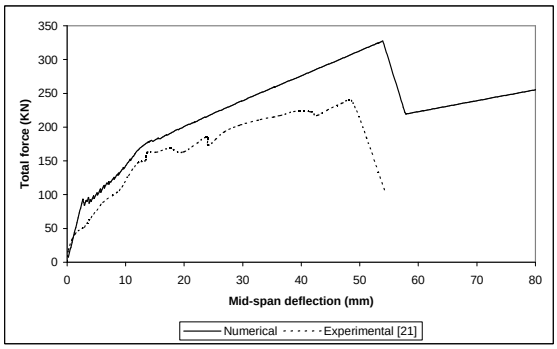

Figure 6: T-beam - Total load x deflection; comparison of experimental and numerical results.

Final failure load and progressive damage are reasonably well represented by numerical model. The failure of de beam was due to delamination of the CFRP layer [21], effect that is not represented by the model.

7.4 Analysis of rectangular reinforced concrete beams strengthened by composite material

a) Fig. 7 shows beam geometry, cross section and loading. The steel bars are represented by plates with equivalent cross-section area. For the progressive failure analysis the Maximum strain criterion was used and the results are compared with those in [4]. The used mesh has 30 eight node elements and 125 nodes.

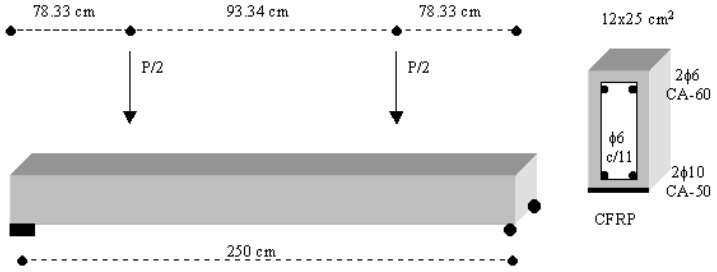

Figure 7: Geometry, cross section e loading

The materials properties are as follows:

- Concrete: average compression strength: 32.8MPa, ultimate strain: 0.3%.
- Upper steel CA50: failure stress: 747.2MPa, yield stress: 587.0MPa.
- Lower steel CA50: failure stress: 800.2MPa, yield stress: 706.5MPa.
- Replark - Mitsubishi Chemical Corporation [4] - E= 230.0GPa, failure strain: 0.0144.

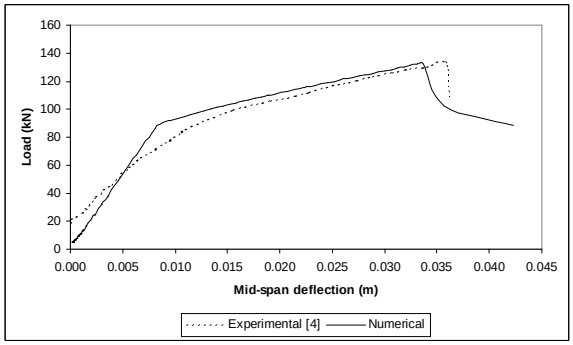

Figure 8: Mid-span deflection; comparison of experimental and numerical results

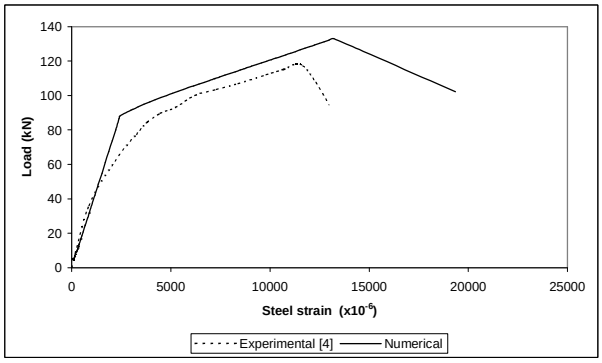

Figure 9: Steel strain at mid-span; comparison of experimental and numerical results

Fig. 8 and 9 show that progressive failure and steel strain are fairly well represented by the numerical model.

b) Fig. 10 shows beam geometry, cross section and loading. The steel bars are represented by plates with equivalent cross-section area. The used mesh has 30 eight node elements and 125 nodes.

The materials properties are as follows:

- Concrete: E= 38.3Gpa, ultimate strain: 0.3%
- Upper steel CA60B: Es=210GPa, yield stress: 738MPa
- Lower steel CA50A: Es=210GPa, yield stress: 565MPa
- Carbon fiber reinforced polymeric plates – CFRP [1]: E= 230GPa, ultimate strain: 0.0148.

The stiffness loss due to the failure of the tensioned concrete layers can be observed (Fig. 11 and 12). In the representation of the steel strain the yielding of the lower steel is perceived (565 MPa). In the experiment, the failure of the composite leads to steel yielding.

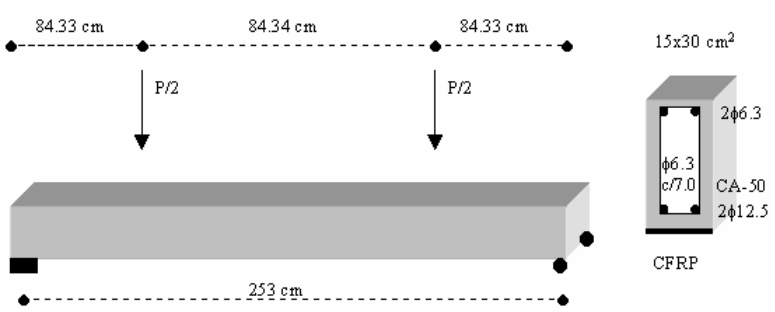

Figure 10: Geometry, cross section e loading

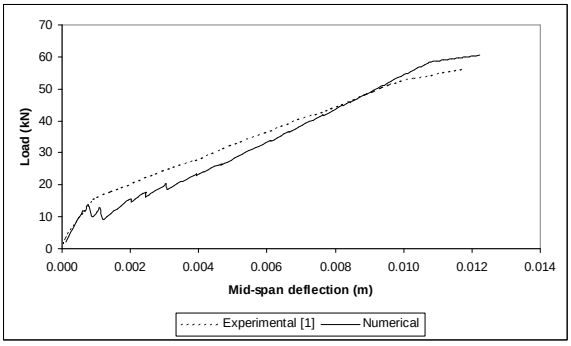

Figure 11: Mid-span deflection

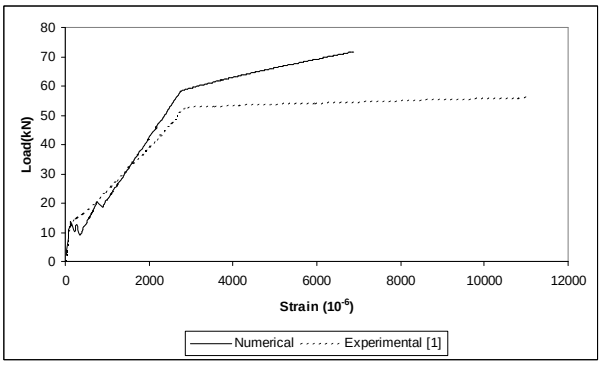

Figure 12: Lower steel strain at mid-span

8 Conclusions and final remarks

The first two examples establish the accuracy and robustness of the model.

The results for the T-beam strengthened with composite material plates show a good agree-

ment for deflections and failure load implying that the adopted failure criterion (Maximum Strain) is adequate to evaluate the initial and final failures of the structure.

From the results for the rectangular beams we have:

1. The load-deflection plot shows that the used degradation criteria represent adequately the experimental behavior. Still, we are working to improve this results using a criterion based on the theory of the Continuum Damage Mechanics.

2. A good estimate of failure loads was obtained.

Although the code has others criteria, we use the Maximum Strain criterion due to the experimental data supplied in [22].

It should be noticed that the finite element code developed is general and allows the analysis of more complex structural types as plates and shells, as well as the calculation of deferred deformations.

Acknowledgements: The financial support of CNPq, CAPES, PROPESQ/UFRGS, UNOCHAPECÓ and the suggestions given by the referees are gratefully acknowledged.

References

[1] M. Aurich. Modelo de ligação entre concreto e armadura na análise de estruturas de concreto pelo método de elementos finitos. *Dissertação de Mestrado em Engenharia (Estruturas)-PPGEC/UFRGS*, 2001.

[2] E. J. Barbero. *Introduction to Composite Materials Design*. Taylor and Francis, Philadelphia, PA, 1998.

[3] K. J. Bathe. *Finite Element Procedures*. Englewood Cliffs N.J.: Prentice-Hall, 1996.

[4] A. J. Beber. Comportamento estrutural de vigas de concreto armado, reforçadas com compósitos de fibra de carbono. *Tese de Doutorado em Engenharia (Estruturas)-PPGEC/UFRGS*, 2003.

[5] M. S. Cheung, G. Akhras, and W. Li. Progressive failure analysis of composite plates by the finite strip method. *Computer Methods in Applied Mechanics and Engineering*, 124(1-2):49–61, 1995.

[6] P. H. Emmons, A. M. Vaysburd, and J. Thomas. Strengthening concrete structures, part ii. *Concrete International*, 20(4):56–60, Apr.1998.

[7] P. H. Emmons, A. M. Vaysburd, and J. Thomas. Strengthening concrete structures, part i. *Concrete International*, 20(3):53–58, Mar. 1998.

[8] L. J. Hart-Smith. The role of biaxial stresses in discriminating between meaningful and illusory composite failure theories. *Composite Structures*, 25:3–20, 1993.

[9] Z. Hashin. Failure criteria for unidirecional fiber composites. *Journal of Applied Mechanics*, 47:329–334, June 1980.

[10] T. J. R. Hughes. *The finite element method*. Englewood Cliffs, N.J.: Prentice-Hall, 1987.

[11] V. M Karbhari and L. Zhao. Use of composites for 21st century civil infrastructure. *Computer Methods Applied Mech. Engrg.*, pages 433–454, 2000.

[12] J. D. Lee. Three dimensional finite element analysis of layered fiber-reinforced composite materials. *Computers & Structures*, 12(3):319–339, 1980.

[13] J. D. Lee. Three dimensional finite element analysis of damage accumulation in composite laminate. *Computers & Structures*, 15(3):335–350, 1982.

[14] Fyfe Co. LLC. *Design manual for Tyfo Fibrwrap System—-Rev.1.* San Diego, CA, USA, 1988.

[15] S. P. C. Marques and G. J. Creus. Geometrically nonlinear finite elements analysis of viscoelastic composite materials under mechanical and higrothermal loads. *Computers and Structures*, 53(2):449–456, 1994.

[16] T. Norris, H. Saadatmanesh, and M. R. Ehsani. Shear and flexural strengthening of r/c beams with carbon fiber sheets. *Journal of Structural Engineering*, 123(7):903–911, July 1997.

[17] B. F. Oliveira and G. J. Creus. Nonlinear viscoelastic analysis of thin-walled beams in composite material. *Thin-Walled Structures*, 41:957–971, 2003.

[18] B.F. Oliveira and G. J. Creus. Viscoelastic failure analysis of composite plates and shells. 49(4):369–384, 2000.

[19] J. C. Simo and T. J. R. Hugues. *Computational Inelasticity*. Springer-Verlag, New York, 1998.

[20] S. Tolson and N. Zabaras. Finite element analysis of progressive failure in laminated composite plates. *Computers & Structures*, 38(3):361–376, 1991.

[21] Dr.Yung-Chih Wang. *Department of Civil Engineering, National Central University, Chung-li, Taiwan 320, Taiwan, ROC*. Personal communication, Aug. 2004.

[22] Y. C. Wang and C. H. Chen. Analytical study on reinforced concrete beams strengthened for flexure and shear with composite plates. *Composite Structures*, 59:137–148, 2003.

[23] Y. B. Yang and M. S. Shieh. Solution method for nonlinear problems with multiple critical points. *AIAA Journal*, 28(12):2110–2116, 1990.